Progress In Electromagnetics Research B, Vol. 103, 37–53, 2023

A Torque Ripple Suppression Strategy for Hysteresis Segmented PWM-DITC Permanent Magnet Assisted Switched Reluctance Motor

Chaozhi Huang, Lixiang Dai*, Yuliang Wu, and Yanwen Sun

Abstract—In the traditional Direct Instantaneous Torque Control (DITC) strategy for permanent magnet assisted switched reluctance motors, the hysteresis control mode during the commutation phase and single-phase on-period is not smooth, resulting in excessive synthetic torque ripple. In this paper, we analyzed this problem, combined with the principle of hysteresis segmentation control and pulse width modulation (PWM), and proposed a hysteresis segmented PWM-DITC strategy. By analyzing the torque error changes in each division area of the inductor, the torque error is adjusted by the internal hysteresis loop during the commutation period and single-phase on-period, so that the hysteresis control is smoother, and the torque ripple is reduced. At the same time, the linear model of rotor angle and inductance is established; the PWM voltage modulation calculation formula at both ends of the winding is calculated and derived; the hysteresis output signal at the commutation time and the single-phase on-time is optimized to further suppress the torque ripple. Finally, through simulation and experimental demonstration, the proposed hysteresis loop segmented PWM-DITC strategy can overcome the problem of unsmooth hysteresis control mode and can effectively suppress torque ripple.

1. INTRODUCTION

Permanent magnet auxiliary switched reluctance motor (SRM) has the advantages of simple structure, low manufacturing cost, and reliable operation, and there is no problem of motor demagnetization caused by high temperature, which has attracted widespread attention, as shown in Figure 1 [1–3]. Due to the unique properties of SRM, there is great potential in electric vehicle transmission. However, the operating capacity of SRM is closely related to the motor topology and control mode, and the performance of motor efficiency, torque ripple, noise, and vibration is different under different control strategies. The opening angle and closing angle of the motor are affected by the excitation phase current, and the corresponding pulse-width modulated voltage signal needs to be controlled [4, 5]. The motor has a large torque ripple during stable operation, and the traditional control method cannot develop the motor performance.

In order to solve the problem of excessive torque ripple, scholars have studied many methods in depth. Reference [6] proposes a smooth pulse width modulation technique to control the voltage change rate during commutation, thereby reducing the noise and vibration of the motor. In [7], the authors use the relationship between PI and shot controller to improve the internal sampling method to avoid PWM signal delay. In [8], the authors adaptively process the single-phase excitation signal in a commutation period by using the idea of model prediction on the basis of non-differential beat control. In [9], the author proposes a PWM signal controller with compensation correction, which reduces the error with

Received 19 June 2023, Accepted 6 September 2023, Scheduled 14 October 2023
* Corresponding author: Lixiang Dai (1583874234@qq.com).
The authors are with the College of Electrical and Automation, Jiangxi University of Science and Technology, Ganzhou 341000, China.

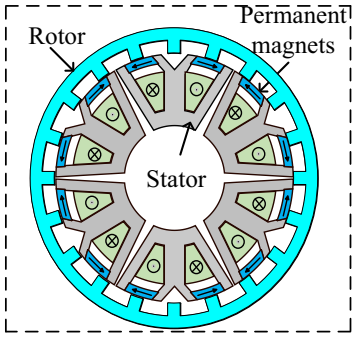

Figure 1. Permanent magnet auxiliary switched reluctance motor (external rotor).

fast response when the hysteresis error is large. When the error is small, PWM solves the torque error in the strategy. In [10], the authors propose a current model-based prediction to predict the pulse cycle duty cycle of the reference current. In [11], in order to ensure the accuracy of current sampling, two sets of current sensors are selected to track the PWM voltage signal to obtain single-phase current and improve the output performance of torque. In [12], in order to limit the high torque ripple of the motor, a new commutation control strategy is proposed, which defines the position-angle relationship and operation mode of the adjacent rotor, and the operation of the two position angles can be well optimized online by genetic algorithm in the operation of high torque and low torque, so as to suppress the torque ripple of the motor. In [13], the authors convert the torque estimation to the form of flux and current, and use the hysteresis controller to output digital voltage to control the instantaneous torque. In [14], according to the characteristics of SRM inductance, the authors construct the turn-on angle function to track the torque while suppressing excessive phase current peaks, and select the provided torque with a large torque-to-current ratio during the commutation period to achieve efficient suppression of torque ripple. In [15], the authors combine adaptive control with DITC to automatically adjust and compensate for torque error, realize the control of motor commutation, and effectively suppress torque ripple. In [16], compared with many commutation compensation strategies, the authors choose to introduce PWM control in the DITC strategy, rely on PWM signals to adjust the torque error, analyze the commutation torque characteristics, and then compensate to suppress torque ripple. In [17], in order to suppress the torque ripple of the motor, the authors process the PWM signal in segments, combine the pulse width modulation technology, analyze the inductance model to obtain the optimal voltage duty cycle, change the voltage at both ends of the excitation winding and the demagnetization winding, and then reduce the torque ripple. In [18], the authors derive the relationship among voltage, current, and inductance in the small inductance region and inductor rising region, obtain a suitable PWM duty cycle signal, adjust the voltage across the motor winding, and realize accurate control of current. In [19], in order to optimize the hysteresis control mode, the authors redivide the inductor region into hysteresis control modes corresponding to different regions, and the angle optimization is more reasonable to improve the motor performance. In [20], the authors use the idea of the ratio of maximum torque current to analyze the change trend of the inductance model, divide the new region and conduction rule, and obtain the ideal PWM voltage duty cycle to reduce the torque ripple of the motor. In [21], in order to suppress the motor torque ripple under the PWM-DITC control strategy, the authors divide the sector into nine and adjust the control mode of the hysteresis loop, and then obtain a new conduction rule and the best PWM voltage signal to control the motor and effectively suppress the motor torque ripple.

The premise of suppressing torque ripple in the above strategy is that the current control is based on the PWM algorithm, which is difficult. Due to the problem of unsmoothing in the hysteresis control in the SRM direct instantaneous torque control strategy (DITC), the output performance of torque during commutation is seriously affected. Aiming at the problem of unsmooth hysteresis control, combined with the relationship between inductance and rotor angle during commutation period and single-phase on-period, this paper designs a segmented smooth hysteresis control method, calculates the inductance change to derive the calculation formula of pulse voltage width, and obtains the optimal voltage signal to drive the motor, effectively solve the problem of unsmooth hysteresis control, and further suppress torque ripple.

2. TRADITIONAL DITC STRATEGY

2.1. Traditional DITC Principle

According to Figure 2, the SRM direct instantaneous torque control strategy consists of hysteresis control, sector division, torque estimation, power converter, and position sensor. The DITC strategy adjusts the output hysteresis signal according to the position detection feedback signal and the error between the reference torque and actual feedback torque, and the power converter executes the command corresponding to the voltage vector table to adjust the winding voltage to control the motor operation.

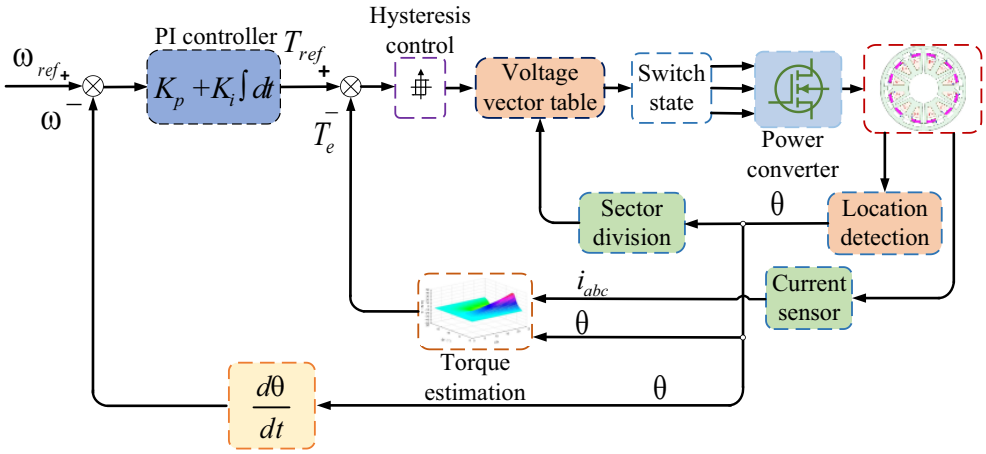

Figure 2. Block diagram of traditional DITC policy.

2.2. Asymmetric Half-Bridge Circuit

There are three switching states of the power converter, namely the excitation state, freewheeling state, and demagnetization state, as shown in Figure 3. When the upper and lower bridge arms are on at the same time, it is recorded as the state $U = 1$; the voltage is applied at both ends of the winding; and the phase is excitation. When the upper side arm is turned off, and the lower side arm switch and diode are on, it is recorded as state $U = 0$, and no voltage is applied at both ends of the winding, which is the freewheeling state. Similarly, when the upper and lower legs are turned off, and the diode is in the reverse conduction condition, it is recorded as state $U = -1$, and the negative voltage applied across the winding is the phase demagnetization state.

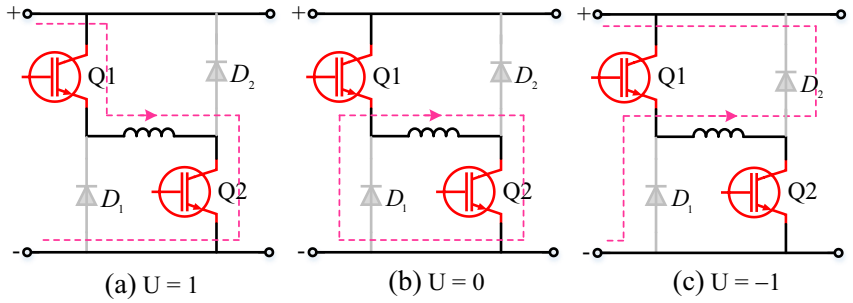

Figure 3. Asymmetric half-bridge switching state.

2.3. Hysteresis Control

Figure 4(a) shows two-phase exchange region, torque hysteresis control method of demagnetization phase and excitation phase. Figure 4(b) is a single-phase conduction region. Red is an excitation phase hysteresis loop, and blue is a demagnetized phase hysteresis loop. $-T_{\max} \sim T_{\max}$ is the external hysteresis loop value, and $-T_{\min} \sim T_{\min}$ is the internal hysteresis loop value, set to torque error. Then there is

$$\Delta T = T_{ref} - T_e \tag{1}$$

where T_{ref} is the reference torque and the actual electromagnetic torque. The traditional DITC strategy adopts the internal hysteresis loop to control the excitation phase state, the external hysteresis loop to control the demagnetization phase state, and the torque error is adjusted through the internal hysteresis loop when the single-phase conduction is on. When the torque error exceeds the external hysteresis loop area, the phase output negative voltage motor winding is demagnetized, so that the motor torque is rapidly reduced.

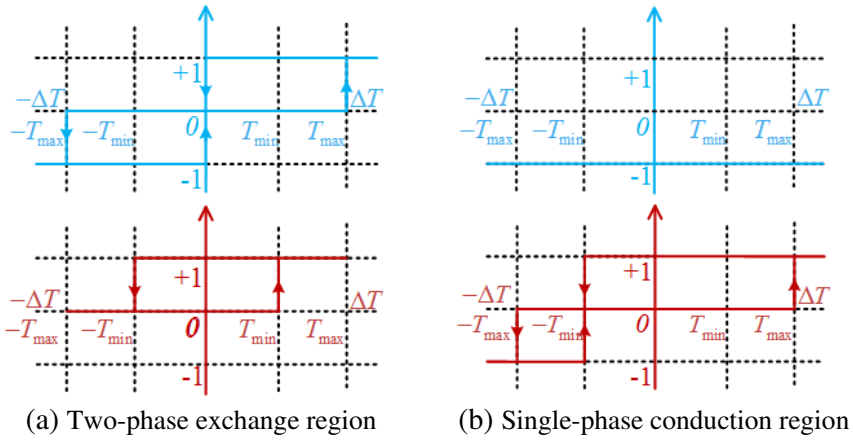

(a) Two-phase exchange region (b) Single-phase conduction region

Figure 4. Traditional DITC policy hysteresis control mode.

The torque error of the traditional hysteresis control strategy changes with the position and time of the motor stator and rotor. When the phase is exchanged, the inductance value of the excitation phase winding is minimal, and the current change rate is large; the current peak is easy to occur; the torque error is affected by the external hysteresis loop of the excitation phase; and the torque error must exceed the external hysteresis loop area. At this time, the motor will have a large torque ripple. At the single-phase on-time, the current tends to be stable, and the torque ripple decreases. The traditional DITC strategy does not consider whether the torque output capacity of the excitation phase and demagnetized phase is stable at the commutation time and still follows the control idea of a single phase in the commutation region, resulting in that the hysteresis control cannot be smoothly transitioned, resulting in large torque ripple.

3. HYSTERESIS SEGMENTED PWM-DITC STRATEGY

Through the above analysis, it is concluded that the control transition between the single-phase on-period and commutation period hysteresis is not smooth, resulting in excessive torque ripple in the exchange phase. A hysteresis segmented PWM-DITC strategy is proposed to improve the hysteresis control mode of the two-phase exchange zone, and the hysteresis segment control principle is used to analyze the inductance and rotor angle changes in the commutation period and single-phase on-period, and derive and calculate the appropriate PWM voltage duty cycle signal to adjust the motor winding voltage as shown in Figure 5.

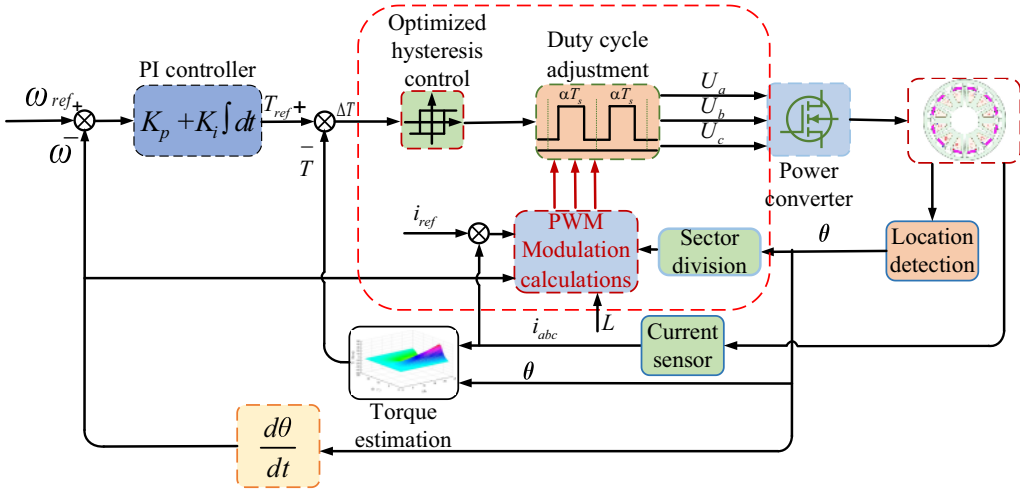

Figure 5. Block diagram of the hysteretic segment PWM-DITC policy.

3.1. New Hysteresis Control

The method divides the commutation period and on-period into four regions. I and II are the two-phase exchange region. The torque output maximum phase is adjusted by the internal hysteresis loop, and the winding with a small torque output is given to the excitation voltage and enters the excitation state. III and IV are single-phase conduction region, which are the ability of the motor to adjust torque before the maximum inductance. When the torque output is low, zero voltage is applied to the winding to enter the freewheeling state, and when the inductance value is at the maximum, a negative voltage is applied to the winding phase after this position to enter the demagnetization state.

According to Figure 7, taking the commutation process between demagnetized phase C and excitation phase A as an example, θ_{off}^{C} is the alternating nodes of region I and region II that are located. In region I, the C phase inductance change rate is large, and the winding phase current is also large enough, but the A phase inductance change rate is basically almost zero. At this moment, C phase bears the responsibility of torque output. Using Figure 6(a) new hysteresis control mode, blue is the demagnetization phase; red is the excitation phase; the working state of the current conduction phase is adjusted by the inner loop, so that the torque error changes in the internal hysteresis loop region. According to the conduction sequence A correspondingly, when the fast excitation maintains the motor torque output, the hysteresis state at this moment is "+1", and when the torque error is less than the external hysteresis limit, the hysteresis state output is "0" state, reducing the output of torque and reducing torque ripple.

$\theta_{off}^{C} \sim \theta_3$ is region II. At this moment, the A phase winding is excitation state; the inductance change rate increases; the current rises; the torque output capacity is enhanced; the C phase begins to demagnetize; the current decreases; the torque output capacity of the motor decreases; and the A phase bears the torque output of the motor. At this moment, the new hysteresis control method of Figure 6(b) is adopted; the torque error in this area is adjusted by the inner loop of phase A; the adjustment range is between the inner hysteresis loop and the outer hysteresis ring region; and the working state of the hysteresis loop of phase C is "−1" or "+1".

$\theta_3 \sim \theta_4$ is region III. At this moment, the C phase inductance change rate gradually decreases until the alignment position becomes zero; A phase inductance change gradually increases; using the hysteresis control strategy shown in Figure 6(c), at this moment the torque error of phase A is still adjusted in the internal hysteresis loop region; C is correspondingly in the demagnetization state; hysteresis working state is "−1". When the torque error is greater than the outer hysteresis loop, the hysteresis output state is "0", compared with the traditional hysteresis mode, and the segmented hysteresis still has the ability to adjust the torque.

$\theta_4 \sim \theta_5$ is the task of region IV, where phase A provides the torque output at this moment, and

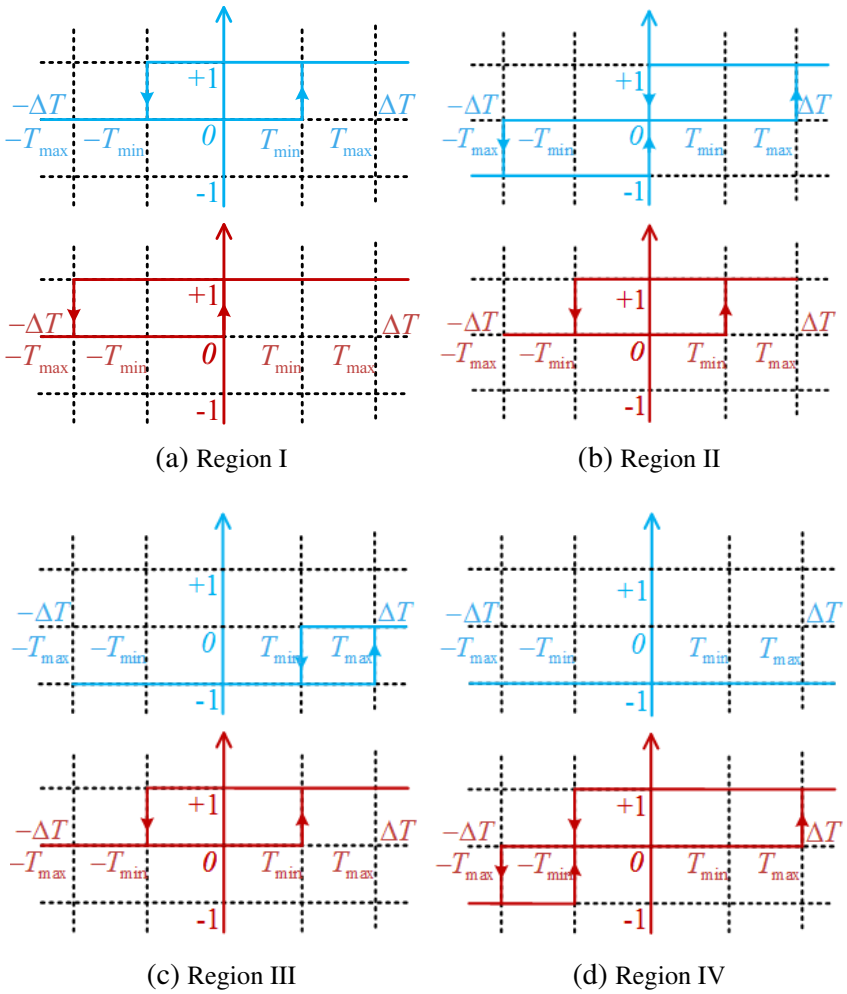

Figure 6. Analysis diagram of hysteresis segment control.

the phase C hysteresis loop is in the "−1" state, as shown in Figure 6(d). At this moment, the torque error changes in the hysteresis loop region, and when the torque error is greater than the hysteresis loop region, the A phase hysteresis loop turns to "−1".

Since the SRM motor has nonlinear characteristics and is related to inductance and combined with the analysis of the linear model diagram, assuming that the current is independent of the winding current, ignoring the magnetic circuit saturation and magnetic field diffusion conditions, the change relationship among the stator, rotor, and angle is shown in Figure 7.

The stator salient pole in the θ_1 position corresponds to the rotor groove, where the inductance is minimal, and the inductance change rate is zero. θ_2 corresponds to the position where the rear edge of the stator is aligned with the front edge of the rotor; θ_3 is the coincidence alignment position of the front edge of the stator and rotor; the inductance in the $\theta_2 \sim \theta_3$ interval rises; the inductance rate of change increases; and the position inductance value is the largest.

$$L(\theta) = \begin{cases} L_{\min} & \theta_1 \le \theta \le \theta_2 \\ K(\theta - \theta_1) & \theta_2 \le \theta \le \theta_3 \\ L_{\max} & \theta_3 \le \theta \le \theta_4 \\ L_{\max} - K(\theta - \theta_4) & \theta_4 \le \theta \le \theta_5 \end{cases} \tag{2}$$

In Equation (2), θ is the rotor angle, $L_{\max}$ the maximum inductance, K the minimum inductance, which can be obtained from the linear model of inductance and rotor position in Figure 7, and the

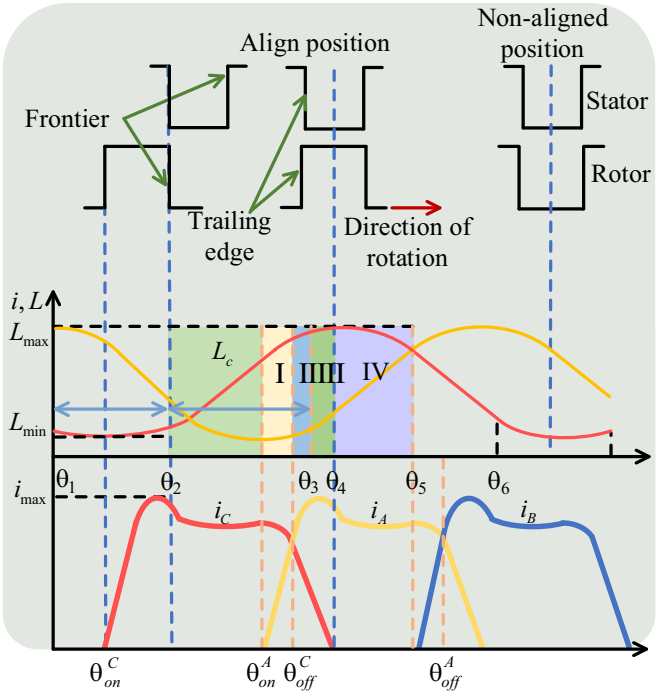

Figure 7. Schematic diagram of inductance, rotor position, and current.

calculation equation is

$$K = \frac{L_{\max} - L_{\min}}{\theta_3 - \theta_2} \tag{3}$$

Similarly, ignoring the saturation condition of the magnetic circuit can obtain the ideal electromagnetic phase torque formula

$$T_k = \frac{1}{2} i_k^2 \frac{dL_k(\theta)}{dt} \tag{4}$$

The total electromagnetic torque is

$$T_{\text{total}} = \sum_{k=1,2,3}^{3} T_k(\theta, i_k) \tag{5}$$

According to the SRM torque characteristics, the instantaneous torque of the motor winding is related to the magnitude of the phase current and the change of inductance at the position. In order to further reduce the torque ripple during the commutation phase of SRM, a control strategy needs to be analyzed and developed for the inductance change characteristics. According to Figure 7, it can be seen that the larger the winding current is, the more serious the saturation characteristics of the inductor are. The rate of inductance change varies periodically with the rotor position, and the phase torque also changes with the rotor position in combination with Equation (4). When the phase current does not change, the instantaneous torque output is proportional to the rate of change in inductance. According to the torque capacity of the motor rotor in different positions, different hysteresis control strategies are adopted to adjust the output PWM voltage signal, which can reasonably reduce the torque ripple.

3.2. $\theta_1 \sim \theta_2$ Interval PWM Modulation Calculation

The relationship between the position of the stator and rotor of the motor and the current is analyzed. The motor phase current is assumed to be independent of the inductance. The influence of magnetic circuit saturation and magnetic field diffusion loss is ignored, and the rotor position and winding inductance change periodically.

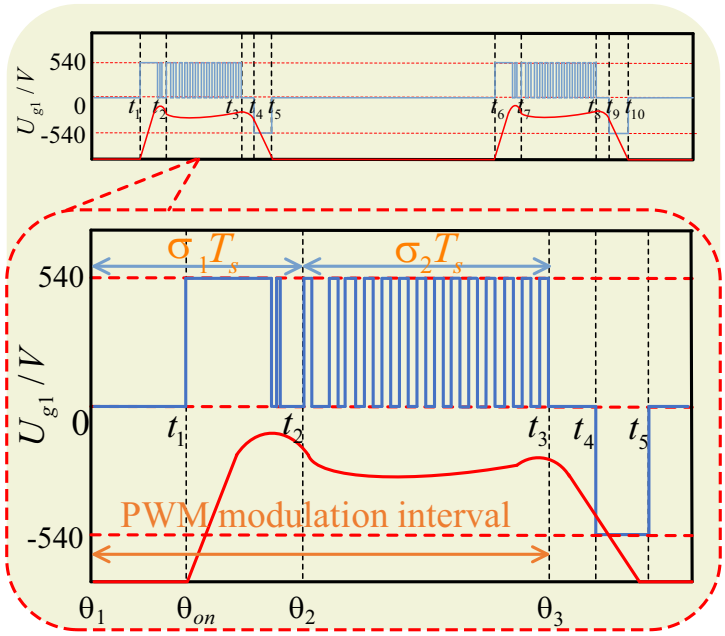

Figure 8. PWM modulation signal analysis diagram.

In Figure 8, $\theta_1 \sim \theta_2$ interval is the two-phase exchange zone. When the rotor position is located in this interval, the inductance value of the excitation phase winding changes little, and it is independent of the excitation phase current. It can be seen from Equation (6) that in this $\theta_1 \sim \theta_2$ interval, the motor torque output is approximately zero. Ignoring motor winding losses, the windings are required to reach a given current at exactly θ_2. It can be known from the SRM phase winding voltage equation

$$U_k = i_k R_k + \frac{d\varphi}{dt} = i_k R_k + L_k \frac{di}{dt} + i_k \frac{dL_k}{dt} \tag{6}$$

Since the inductance value remains essentially constant in the $\theta_1 \sim \theta_2$ interval, the inductance curve is approximately zero and is denoted as $L_{\min}$, and $\omega = 2\pi n$, then Equation (6) can be treated as

$$U_k = i_k R_k + L_k \frac{di_k}{dt} = i_k R_k + L_{\min} \omega \frac{di_k}{d\theta} \tag{7}$$

$$U_k = i_{ref} R_k + \frac{L_{\min} \pi n}{30} \frac{di_k}{d\theta} \tag{8}$$

When the turn-on angle is θ_{on}, the inductance remains unchanged in the $\theta_1 \sim \theta_2$ range, and solving Equation (6) yields that the current i_k is

$$i_k(\theta) = \frac{30 \int_{\theta_1}^{\theta_2} (U_k - i_k R_k) dt}{L_{\min} \pi n} \tag{9}$$

Taking phase A as an example, when the rotor rotates from the non-aligned position to the aligned position, after the $\theta_1 \sim \theta_2$ interval, the voltage across the lowest winding of the inductor is extremely small and negligible, then the current corresponding to the θ_2 position is

$$i_k(\theta_2) = \frac{30 \int_{\theta_1}^{\theta_2} U_k dt}{L_{\min} \pi n} = \frac{30(\theta_2 - \theta_1) U_k}{L_{\min} \pi n} \tag{10}$$

The winding inductance remains basically unchanged at the $\theta_1 \sim \theta_2$ position, and the k-phase winding circuit can be equivalent to a series RL first-order circuit. i_k is the given reference current

value. Substituting $i_{ref} = i_k$ into Equation (10) and solving for it

$$U_{k1} = \frac{i_{ref} L_{\min} \pi n}{30(\theta_2 - \theta_1)} \tag{11}$$

Let the SRM winding voltage be U_d and the PWM signal width in the $\theta_1 \sim \theta_2$ range be U_k/U_d and denoted as δ_1

$$\delta_1 = \frac{i_{ref} L_{\min} \pi n}{30(\theta_2 - \theta_1) U_d} \tag{12}$$

The $\theta_1 \sim \theta_2$ interval corresponds to the $0 \sim t_2$ interval, then the inductance $L_{\min}$ is

$$L_{\min} = \frac{\int_0^{t_2} U_k dt}{i_k(\theta_1)} \tag{13}$$

The voltage in the $0 \sim t_2$ range is the number of times in the PWM period of the on-power device, from which Equation (12) can be discretized.

$$L_{\min} = \frac{n_1 U_d T_{PWM}}{i_k(\theta_1)} \tag{14}$$

where n_1 is the number of PWM cycles of the conduction power device in the $0 \sim t_2$ range.

3.3. $\theta_1 \sim \theta_2$ Interval PWM Modulation Calculation

By analyzing the current of the stator and rotor of the motor in the non-aligned region $\theta_2 \sim \theta_3$ during the single-phase on-period, the current remains unchanged and approximately equal to i_{ref}, and it can be seen that the rate of change of the current for time is zero, and the calculation formula can be obtained

$$U_k = i_k R_k + i_k \frac{dL_k}{dt} = i_{ref} \left(R_k + \omega \frac{dL_k}{d\theta} \right) \tag{15}$$

The same goes for

$$U_{k2} = i_{ref} \left(R_k + \frac{\pi n}{30} \frac{dL_k}{d\theta} \right) \tag{16}$$

The voltage provided across the winding is U_d, and the PWM signal width in the $\theta_2 \sim \theta_3$ range can be obtained as U_k/U_d, which is denoted as δ_2

$$\delta_2 = i_{ref} \left(\frac{R_k}{U_d} + \frac{\pi n}{30 U_d} \frac{dL_k}{d\theta} \right) \tag{17}$$

$\theta_2 \sim \theta_3$ since the inductance curve is approximately straight, and the inductance slope K_L can be known

$$K_L = \frac{dL_k}{d\theta} = \frac{L_k(\theta_2) - L_{\min}}{\theta_2 - \theta_1} \tag{18}$$

Since the reference current is equal to the winding current, $\theta_2 \sim \theta_3$ and $t_2 \sim t_3$ correspond to the time, and the inductance slope K can be expressed as

$$K_L = \frac{\int_{t_2}^{t_3} (U_k - i_k R_k) dt}{i_{ref}(\theta_3 - \theta_2)} \tag{19}$$

Discretize the inductor

$$K_L = \frac{\left(n_2 U_d - R_k \sum_{t=1}^{n_2} i_t \right) T_{PWM}}{i_{ref}(\theta_3 - \theta_2)} \tag{20}$$

where n_2 is the number of PWM cycles of the conduction power device in the interval $\theta_2 \sim \theta_3$, and i_t is the winding current on-time.

4. SIMULATION AND ANALYSIS

In order to verify the effectiveness of the hysteretic segmented PWM-DITC switched reluctance motor control strategy proposed in this paper, the minimum inductance is obtained in the AYANS simulation program to be 0.007 H, and the 6/20 permanent magnet assist (PMa)-SRM simulation model is established on Matlab/simulink. In the simulation experiment, using the traditional DITC strategy as a reference, the given experimental conditions are: speed 400 r/min, 600 r/min, 800 r/min, load 2 N · m, and 4 N · m. The traditional DITC strategy and the hysteresis segmented PWM-DITC strategy are simulated and verified, and the torque waveforms and current diagrams of the two control strategies are compared.

To compare torque ripple between the two strategies, the torque ripple coefficient is defined as K_e, as shown in Equation (21).

$$K_e = \frac{T_{\max} - T_{\min}}{T_{ref}} \times 100\% \tag{21}$$

In the formula, $T_{\max}$ is the maximum torque, $T_{\min}$ the minimum torque, and T_{ref} the reference average torque. The experimental data of the 6/20 PMa-SRM prototype are used, and the prototype parameters are shown in Table 1.

Table 1. 6/20 PMa-SRM prototype parameters.

Parameter	SRM
Number of phases	3
Rated power P_e/kW	16.2
Rated voltage U_e/V	540
Rated current I_e/A	30
Rated speed n_e/(r/min)	1500
Number of stator/rotor poles	6/20
Cooling method	Air cooled

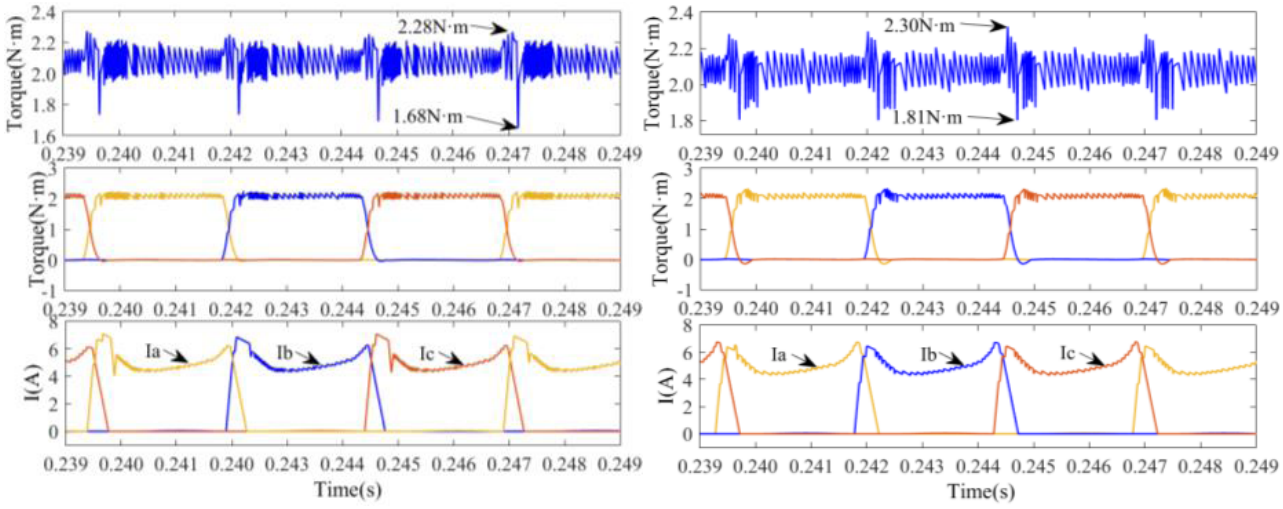

(a) Traditional DITC strategies (b) Hysteretic segmentation PWM-DITC strategy

Figure 9. Torque and current waveforms of traditional DITC strategy and hysteretic segmented PWM-DITC strategy (400 r/min, 2 N · m).

As shown in Figures 9(a) and (b), the torque and current waveforms of the traditional DITC strategy and the hysteresis segmented PWM-DITC strategy are shown at a speed of 400 r/min and a load of 2 N · m. According to the figure, the torque range of the traditional DITC strategy is (1.68 ∼ 2.28) N · m, and the torque ripple rate is 31.50%. Due to the low inductance value during the commutation period, the rising current needs to provide excitation, the initial moment of the excitation phase current fluctuates greatly; the current peak is 7.6 A; the torque range of the hysteresis segmented PWM-DITC strategy is (1.81 ∼ 2.30) N · m; the torque ripple rate is 23.50%; the phase current waveform is smooth; and the current peak is lower. The peak current is 6.9 A.

The above experimental conditions remain unchanged, and the load is increased to 4 N · m, as shown in Figures 10(a) and (b). The traditional DITC strategy torque range is (3.40 ∼ 4.40) N · m; the torque ripple rate is 25.00%; d the phase current will increase with the increase of load; and the peak current is 9.8 A. The hysteretic segment PWM-DITC strategy torque range is (3.81 ∼ 4.30) N · m; the torque ripple rate is 12.25%; and the peak current is 9.4 A.

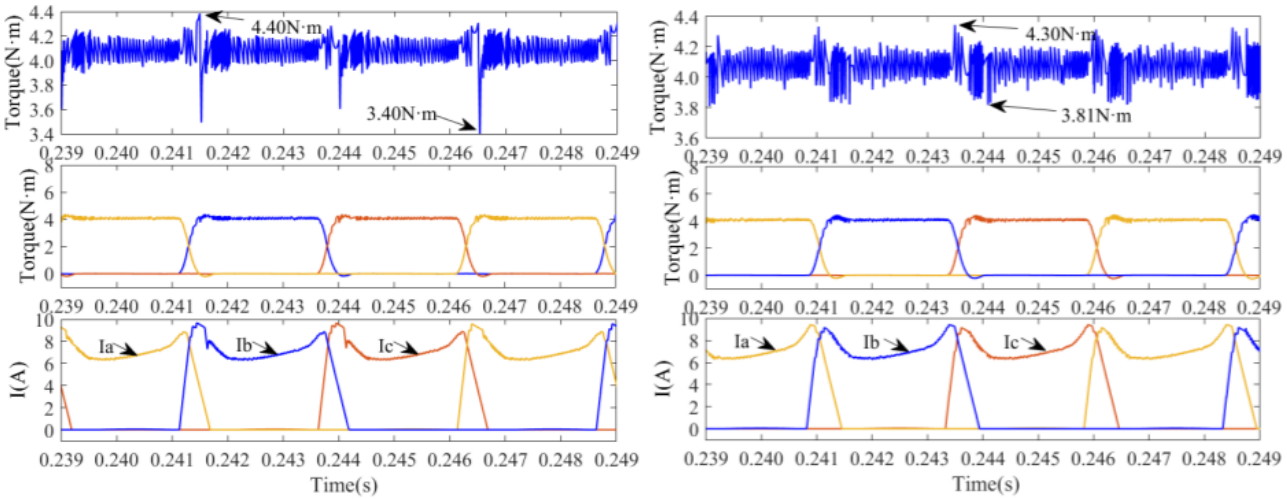

(a) Traditional DITC strategies (b) Hysteretic segmentation PWM-DITC strategy

Figure 10. Torque and current waveforms of traditional DITC strategy and hysteretic segmented PWM-DITC strategy (400 r/min, 4 N · m).

Combined with data analysis, it can be seen that compared with the traditional DITC strategy, the hysteretic segmented PWM-DITC strategy can still effectively suppress the torque ripple during SRM operation under increased load conditions. In order to further verify the effectiveness of the hysteretic segmented PWM-DITC strategy, the torque and current waveforms of the traditional strategy and the hysteretic segmented PWM-DITC strategy under different working conditions are shown below.

According to Figures 11(a) and (b), comparing the current and torque waveforms of the traditional DITC strategy and the hysteresis segmented PWM-DITC strategy, it can be seen that when the speed is 600 r/min, and the load is 2 N · m, the traditional DITC policy torque range is (1.67 ∼ 2.30) N · m; the torque ripple rate is 31.50%; and the phase current peak is 7.5 A. The hysteresis segmented PWM-DITC torque range is (1.90 ∼ 2.31) N · m; the torque ripple rate is 20.50%; and the peak phase current is 6.8 A.

As shown in Figures 12(a) and (b), the load is increased to 4 N · m; the traditional DITC strategy torque range is (3.48 ∼ 4.50) N · m; the torque ripple rate is 25.75%; and the peak phase current is 9.8 A. The hysteretic segmented PWM-DITC strategy torque range is (3.81 ∼ 4.36) N · m; the torque pulse rate is 13.75%; and the peak phase current is 9.2 A. From Figure 11, Figure 12, and Table 2, it can be seen that due to the increase of speed and load, the hysteresis segmented PWM-DITC strategy has a lower current fluctuation and lower current peak than the traditional DITC strategy, and the suppression effect of torque ripple is better.

Similarly, according to Figures 13(a) and (b), when the speed is 800 r/min, and the load is 2 N · m, the traditional DITC strategy torque range is (1.68 ∼ 2.30) N · m; the torque ripple rate is

Table 2. Comparison of current peak and torque ripple rate between traditional DITC strategy and hysteretic segmented PWM-DITC strategy.

Load	Control policies	Rotate speed (r/min)	Torque range (N · m)	Phase current (A)	Torque ripple rate (%)
2 N · m	Traditional DITC	400	1.68 ∼ 2.28	7.6	31.50
		600	1.67 ∼ 2.30	7.5	31.50
		800	1.68 ∼ 2.30	7.6	31.00
	Hysteretic segment PWM-DITC	400	1.81 ∼ 2.30	6.9	23.50
		600	1.90 ∼ 2.31	6.8	20.50
		800	1.91 ∼ 2.31	6.8	20.00
4N·m	Traditional DITC	400	3.40 ∼ 4.40	9.8	25.00
		600	3.48 ∼ 4.50	9.8	25.75
		800	3.47 ∼ 4.51	10.0	26.00
	Hysteretic segment PWM-DITC	400	3.81 ∼ 4.30	9.4	12.25
		600	3.81 ∼ 4.36	9.2	13.75
		800	3.90 ∼ 4.41	9.3	12.75

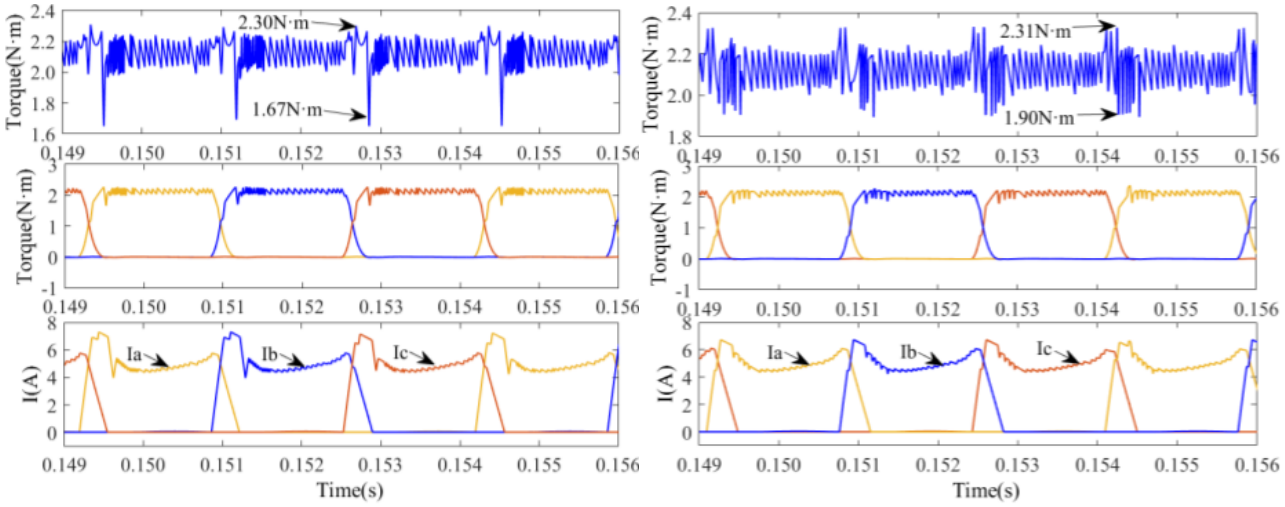

(a) Traditional DITC strategies (b) Hysteretic segmentation PWM-DITC strategy

Figure 11. Torque and current waveforms of traditional DITC strategy and hysteretic segmented PWM-DITC strategy (600 r/min, 2 N · m).

31.00%; and the peak phase current is 7.6 A. The hysteresis segmented PWM-DITC torque range is (1.91 ∼ 2.31) N · m; the torque ripple rate is 20.00%; and the peak phase current is 6.8 A.

As shown in Figures 14(a) and (b), the load is increased to 4 N · m; the traditional DITC strategy torque range is (3.47 ∼ 4.51) N · m; the torque ripple rate is 26.00%; and the peak phase current is 10.0 A. The hysteretic segmented PWM-DITC strategy torque range is (3.90 ∼ 4.41) N · m; the torque pulse rate is 12.75%; and the peak phase current is 9.3 A. Combined with Figure 13, Figure 14, and Table 2 for further analysis, it can be seen that under the same high speed and high load torque, the hysteresis segmented PWM-DITC strategy has a lower phase current peak than the traditional DITC strategy,

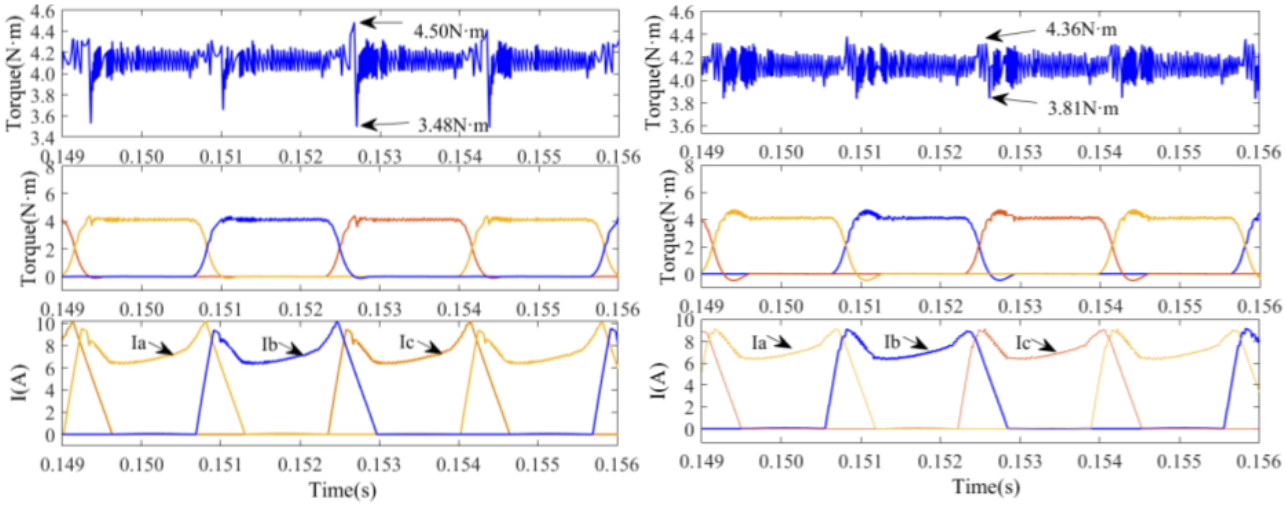

(a) Traditional DITC strategies (b) Hysteretic segmentation PWM-DITC strategy

Figure 12. Torque and current waveforms of traditional DITC strategy and hysteretic segmented PWM-DITC strategy (600 r/min, 4 N · m).

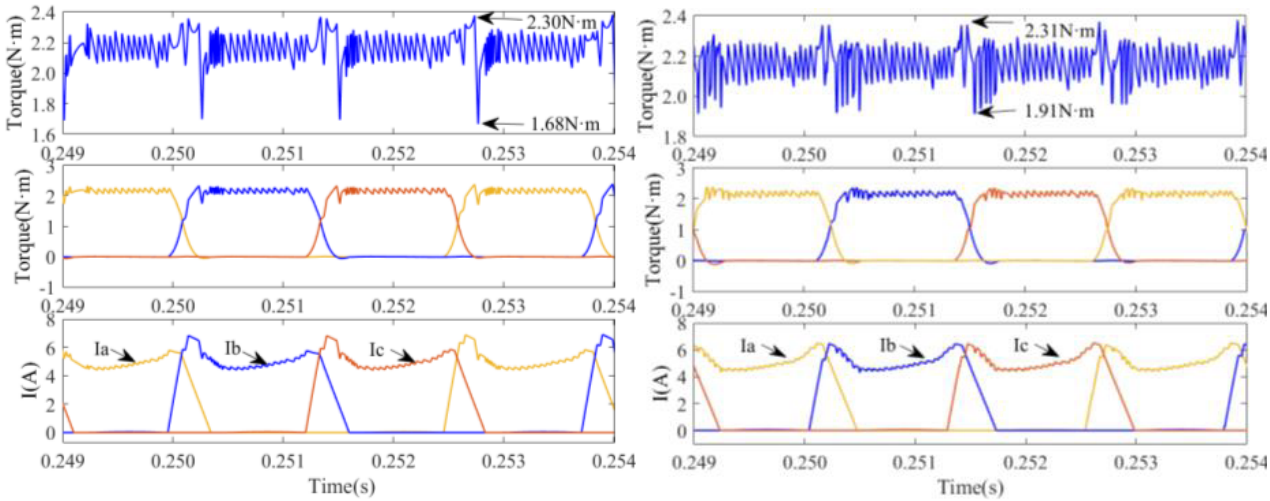

(a) Traditional DITC strategies (b) Hysteretic segmentation PWM-DITC strategy

Figure 13. Torque and current waveforms of traditional DITC strategy and hysteretic segmented PWM-DITC strategy (800 r/min, 2 N · m).

and the suppression effect of torque ripple is good, which is suitable for operation under high load and high torque under the experimental conditions in this paper. The torque ripple during operation is lower, and the torque output performance of the motor is better.

5. EXPERIMENTAL VERIFICATION ANALYSIS

In order to further verify the effectiveness of the hysteretic segmented PWM-DITC strategy, a 16.2 kW experimental prototype test platform was built taking the 6/20 PMa-SRM real sample motor as an example, and the experimental data of the prototype were recorded through the host computer and oscilloscope, as shown in Figure 15. The DSP controller is TMS320F28335 with a sampling frequency

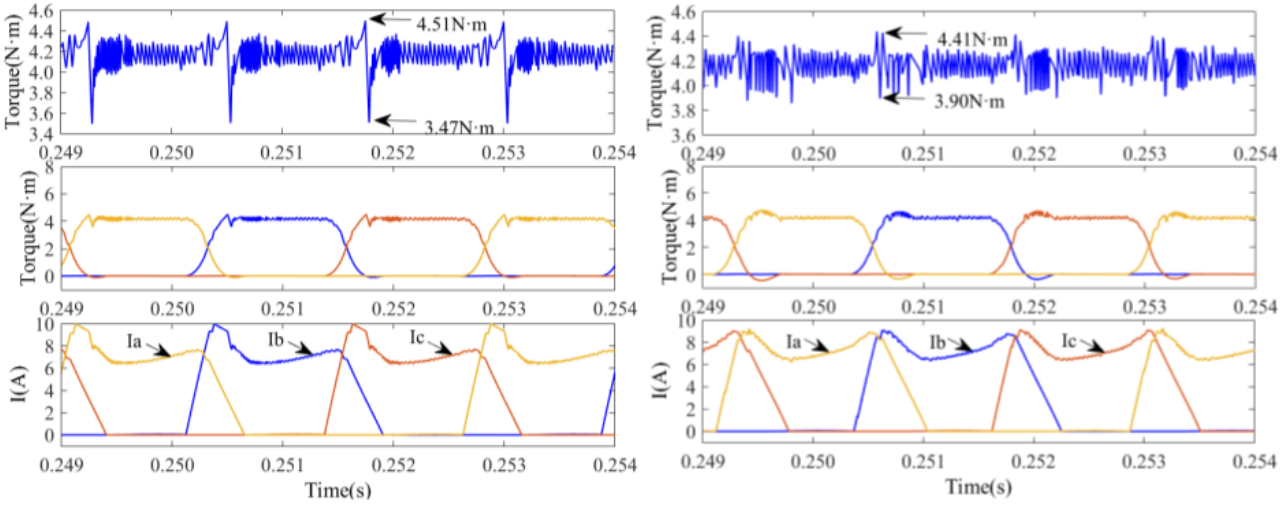

(a) Traditional DITC strategies (b) Hysteretic segmentation PWM-DITC strategy

Figure 14. Torque and current waveforms of traditional DITC strategy and hysteretic segmented PWM-DITC strategy (800 r/min, 4 N · m).

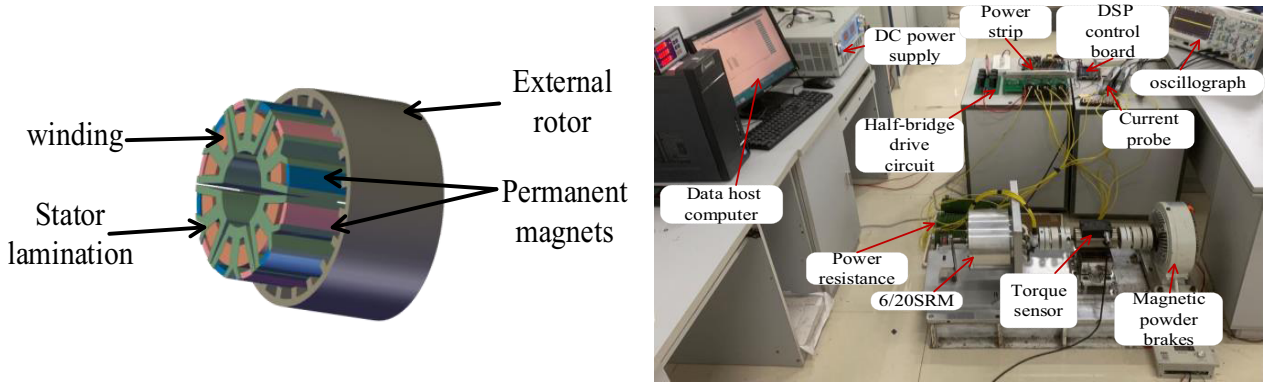

(a) PMa-SRM 3D structure model (b) experimental prototype

Figure 15. PMa-SRM experimental prototype platform (6/20).

of 5 ∼ 15 kHz to realize real-time sampling of SRM torque. The hysteretic segmented PWM-DITC strategy was used for experimental demonstration, as shown in Figures 16 and 17.

According to the experimental results of Figure 16 and Figure 17, when the load is 2 N · m, and the speed is 800 r/min, the torque range of the traditional DITC strategy is (1.70 ∼ 2.41); the current is 7.3 A; the torque ripple is 35.5%; the current waveform is not smooth; and the torque ripple is large. The hysteresis segmented PWM-DITC strategy torque range is (1.81 ∼ 2.30); the peak current is 7.0 A; the torque ripple is 24.5%. At the initial moment, the current waveform is smooth; the change is slow; and the fluctuation is less. Then the current directly enters the off state. Through the analysis, it can be seen that due to the high speed, affected by the delay of the hysteresis loop program calculation time and position sampling time, the torque error is greater than the limit of the hysteresis loop, and the hysteresis loop enters the "0" state, resulting in that the current does not has the same waveform as the simulation and directly enters the off state, in line with the new hysteresis control mode of Figure 6(c).

When the load is 4 N · m, the traditional DITC strategy torque range is (3.40 ∼ 4.52); the current peak is 10.5 A; the torque ripple is 28.0%; the hysteretic segmented PWM-DITC control strategy ripple range is (3.90 ∼ 4.50); the current peak is 9.8 A; and the torque ripple is 15.0%.

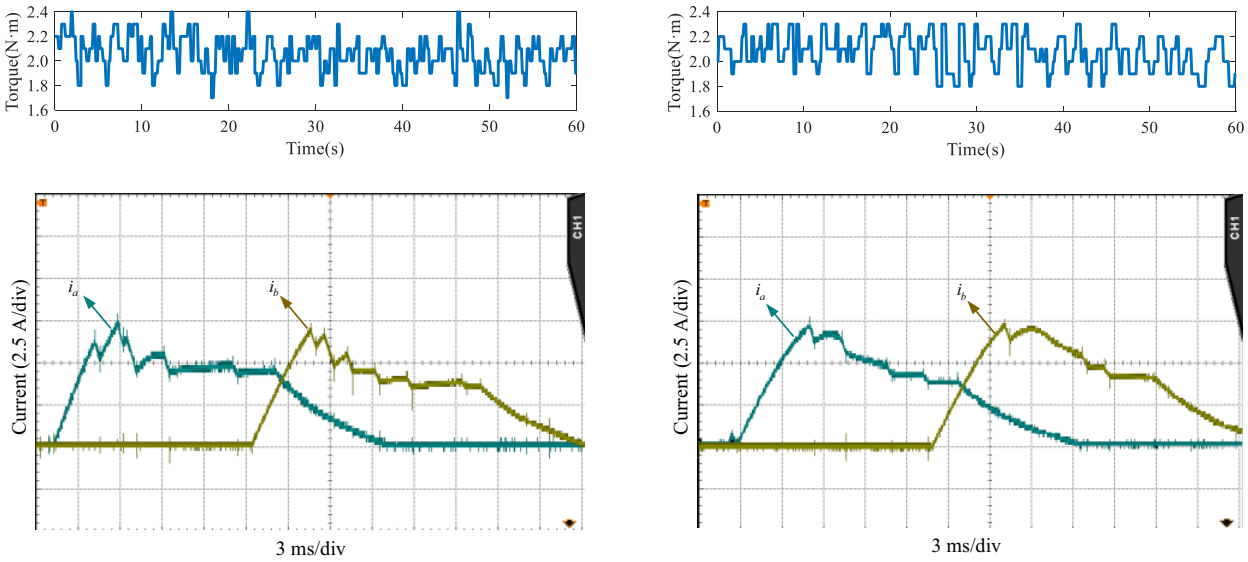

(a) Traditional DITC strategy torque and current waveforms

(b) Hysteresis segmented PWM-DITC strategy torque and current waveform

Figure 16. 800 r/min, 2 N · m traditional DITC strategy and hysteresis segmented PWM-DITC torque and current waveform comparison.

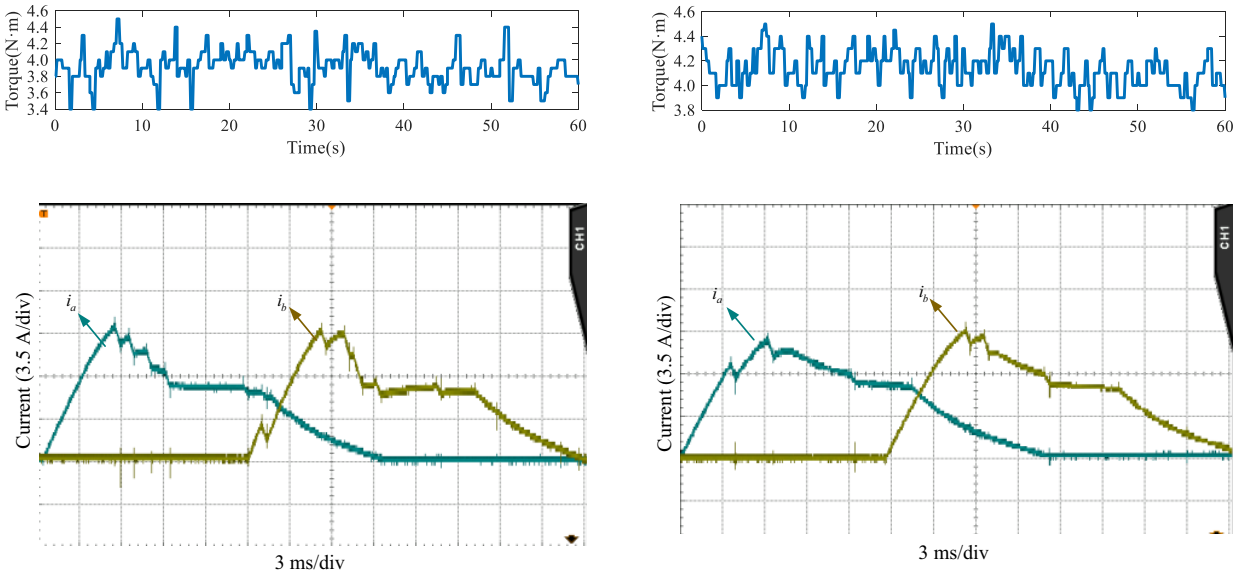

(a) Traditional DITC strategy torque and current waveforms

(b) Hysteresis segmented PWM-DITC strategy torque and current waveform

Figure 17. 800 r/min, 4 N · m traditional DITC strategy and hysteresis segmented PWM-DITC torque and current waveforms.

Ignoring the error of physical experiment and simulation experimental conditions, it can be seen from the analysis of the above platform experiment results that the torque ripple suppression effect of the hysteresis segmentation strategy is better than that of the traditional strategy, which further reflects the practical value of the hysteresis segmentation strategy.

6. CONCLUSIONS

In this paper, a hysteresis segmented PWM-DITC control strategy is proposed for the hysteresis control and torque ripple of switched reluctance motors during commutation. By comparing the current and torque waveforms of the traditional DITC strategy and the hysteresis segmented PWM-DITC strategy through simulation and experiment, it is demonstrated that the hysteresis segmented PWM-DITC strategy has a good effect on solving the problem of unsmooth hysteresis control during commutation. The motor has little dependence on body parameters, is easy to implement, and has good transmission and versatility to SRM control.

The results show that:

(1) In this paper, the hysteresis segmented PWM-DITC strategy is proposed to effectively solve the problem of large torque ripple during commutation caused by unsmooth hysteresis control.

(2) In this paper, the hysteresis segmented PWM-DITC strategy is proposed to reasonably regulate the PWM signal in the commutation period, so that the hysteresis control is smoother and more stable, and the torque ripple of the motor is further suppressed.

ACKNOWLEDGMENT

The study was supported by the National Natural Projects Fund of China, numbered 52167005.

REFERENCES

1. Ma, J., D. Wang, R. Qu, J. Li, and X. Li, "Quasi-three-dimensional analysis and design of an axial flux switched reluctance motor based on grain oriented silicon stee," *Transactions of China Electrotechnical Society*, Vol. 33, No. 17, 4069–4077, Sep. 2018.
2. Gu, Y., Z. Deng, and J. Shao, "A conducting interval optimized sensorless starting method for switched reluctance motor," *Transactions of China Electrotechnical Society*, Vol. 32, No. 19, 11–20, Oct. 2017.
3. Cao, X., H. Hu, N. Yan, and Z. Deng, "Direct torque control of switched reluctance motor with real-time optimization of sectors," *Transactions of China Electrotechnical Society*, Vol. 33, No. 19, 4526–4534, Oct. 2018.
4. Yu, C., Z. Xiao, Y. Huang, and Y. Zhu, "Two-step commutation control of switched reluctance motor based on PWM," *Journal of Engineering*, Vol. 2019, No. 22, 8414–8418, Sep. 2019.
5. Li, B., X. Ling, Y. Huang, and L. Gong, "An improved model predictive current controller of switched reluctance machines using time-multiplexed current sensor," *Sensor*, Vol. 17, No. 5, 1146–1162, May 2017.
6. Pupadubsin, R., B. C. Mecrow, and J. D. Widmer, "Smooth voltage PWM for vibration and acoustic noise reduction in switched reluctance machines," *IEEE Transactions on Energy Conversion*, Vol. 36, No. 3, 1578–1588, Sep. 2021.
7. Fei, P., Y. Jin, and E. Ali, "A digital PWM current controller for switched reluctance motor drives," *IEEE Transactions on Power Electronics*, Vol. 31, No. 10, 7087–7098, 2016.
8. Song, S., J. Liu, Y. Zhao, L. Ge, R. Ma, and W. Liu, "High-dynamic four-quadrant speed adjustment of switched reluctance machine with torque predictive control," *IEEE Transactions on Industrial Electronics*, Vol. 69, No. 8, 7733–7743, Aug. 2022.
9. Cheng, Y., "Modified PWM direct instantaneous torque control system for SRM," *Mathematical Problems in Engineering*, PDF, 1–13, Oct. 2021, https://doi.org/10.1155/2021/1158360.
10. Rajib, M., H. Iqbal, and S. Yilmaz, "A fixed switching frequency predictive current control method for switched reluctance machines," *IEEE Transactions on Industry Applications*, Vol. 50, No. 6, 3717–3726, 2014.
11. Wei, P., G. Johan, A. Jin-Woo, and D. Lee, "Torque sharing function control of switched reluctance machines with reduced current sensors," *CES Transactions on Electrical Machines and Systems*, Vol. 2, No. 4, 355–362, Dce. 2018.

12. Song, S., G. Fang, R. Hei, J. Jiang, R. Ma, and W. Liu, "Torque ripple and efficiency online optimization of switched reluctance machine based on torque per ampere characteristics," *IEEE Transactions on Power Electronics*, Vol. 35, No. 9, 9610–9618, Sep. 2020.
13. Inderk, R. B., W. Rik, and A. A. De Doncker, "DITC — Direct instantaneous torque control of switched reluctance drives," *IEEE Transactions on Industry Applications Industry*, Vol. 39, No. 4, 1046–1051, Aug. 2003.
14. Qing, L., H. Wang, and X. Ge, "A high efficiency torque ripple suppression method for switched reluctance motor," *Transactions of China Electrotehnical Society*, Vol. 35, No. 9, 1912–1920, May 2020.
15. Sun, Q., J. Wu, and C. Gan, "Optimized direct instantaneous torque control for SRMs with efficiency improvement," *IEEE Transactions on Industry Electronics*, Vol. 68, No. 3, 2072–2082, Mar. 2021.
16. Wang, S., Z. Hu, and X. Cui, "Research on novel direct instantaneous torque control strategy for switched reluctance motor," *IEEE Access*, Vol. 8, 66910–66916, Apr. 2020.
17. Ma, M., K. Yuan, Q. Yang, and S. Yang, "Subsection PWM variable duty cycle control of switched reluctance motor based on current soft chopping," *Proceedings of the CSEE*, Vol. 38, No. 18, 5582–5589, Sep. 2018.
18. Tian, D., B. Qu, J. Song, and Y. Zhao, "An analytical method of PWM duty cycle for switched reluctance motors based on current chopping control," *Transactions of China Electrotechnical Society*, Vol. 34, No. 21, 4449–4457, Nov. 2019.
19. Cai, Y., C. Ju, H. Wang, Y, Wan, and H. Zhang, "A new direct instantaneous torque control method of switched reluctance motor and its high efficiency operation," *Transactions of China Electrotechnical Society*, Vol. 37, No. 18, 4625–4637, Sep. 2022.
20. Xu, A., L. Huang, Q. Li, C. Shang, and J. Zhu, "Direct instantaneous torque control optimization of switched reluctance motor for high torque per ampere ratio," *Electric Drive*, Vol. 51, No. 5, 64–69, Aug. 2021.
21. Zhu, Y., G. Zhang, and Y. Huang, "PWM-based direct instantaneous torque control of switched reluctance machine," *Transactions of China Electrotechnical Society*, Vol. 32, No. 7, 31–39, Apr. 2021.